PERGAMON

International Journal of Multiphase Flow 26 (2000) 1369–1400

International Journal of Multiphase Flow

www.elsevier.com/locate/ijmulflow

The structure of two-phase grid turbulence in a rectangular channel: an experimental study

Thrasyvoulos Panidis*, Demosthenes D. Papailiou

Laboratory of Applied Thermodynamics, University of Patras, GR-265 00 Patras, Greece

Received 9 March 1999; received in revised form 8 April 1999

Abstract

Measurements in two-phase, water–air bubble, grid turbulence have been conducted in a vertical water channel of square cross section. The water flow was directed upwards. A 30 mm mesh grid located at the entrance of the test section generated, in the absence of the dispersed phase, a nearly isotropic turbulent flow field occupying the central part of the channel. Air bubbles were injected in the flow from the grid. Velocity measurements of the liquid phase were obtained using Laser Doppler Velocimetry. The measured flow characteristics included mean velocity and statistical quantities such as turbulence intensity, probability distribution function, skewness and flatness factors, autocorrelation, macroscale and power spectra, for both the longitudinal and transverse velocity components. Local void fraction was measured with an optical probe as well as with hot film anemometry. Bubble velocity and size were estimated with photographic techniques. Presented measurements illustrate the upwards development of void fraction distribution at successive cross sections of the channel. The observed distributions indicate the presence of a mechanism responsible for capturing and redistributing the bubbles. Accordingly, physical mechanisms possibly responsible for the observed phenomenon such as a Segre–Silberberg effect, modified for deformable bubbles in the presence of buoyancy, or the action of large eddies present in the flow are discussed. The velocity field has been obtained on a cross-section at a distance of 30 mesh from the grid at a constant water volumetric flow rate. Based on the obtained experimental results, the influence of the dispersed phase on the initially isotropic turbulence field is identified and the physical processes responsible for the observed changes are discussed. The presence of the second phase appears to introduce inhomogeneities in the void fraction and flow property distributions leading to the emergence of two spatial regions controlled by different physical processes. Also, two distinct regimes in the measured quantities are observed, corresponding to low and high values of gas flow rate ratio. The described changes result in a significant departure from initial isotropy, followed by a tendency towards returning to a state characterised by nearly normal probability

* Corresponding author.

PII: S0301-9322(99)00085-3

distributions and scales close to that of grid turbulence as the gas flow rate increases. Finally, the measured autocorrelation and power spectra offer information regarding the nature of the energy exchanging mechanism occurring between the liquid and dispersed phase.

Keywords: Two-phase flow; Bubbly flow; Grid turbulence

1. Introduction

During the last few decades multiphase flows have been the subject of an increasing number of studies, due to the application they find in a wide range of fields in science and engineering. However, at the present time, existing knowledge on the structure of two-phase turbulent flows and the effect of the dispersed phase on turbulence transport processes is lacking considerably behind the accumulated knowledge on single-phase turbulence. It is therefore plausible to suggest that, reaching the same level of understanding already attained in ordinary turbulence is a meaningful objective for planning research on two-phase turbulence.

In this context, following the historic development of research on single-phase ordinary turbulence, the present work constitutes a study regarding the influence of a second dispersed phase on the structure of a simple well investigated turbulent flow that is, the nearly isotropic turbulence field created behind a grid.

Several investigators have performed measurements in liquid–gas bubble two-phase flows. The main topics addressed are the phase distribution, the turbulence structure and the developing wall shear. Most of the conducted experiments refer to up-flows in vertical tubes of which references and their main experimental parameters are given in Table 1. The main conclusions of these experiments are summarised as follows. A 'void peaking' phenomenon according to which bubbles tend to concentrate in the vicinity of the walls was observed. The velocity profile exhibits a wider flat region for low void fraction than the corresponding single-phase profile, while for higher void fraction values it becomes 'dome' shaped. Turbulence intensity measurements show different trends. According to Serizawa et al. (1975) and Wang et al. (1987), the turbulence intensity for low void fraction can become even lower than that corresponding to single-phase at specific locations of the cross section. More important, they found that isotropy is destroyed as longitudinal and transverse intensity values depart. However, Theofanous and Sullivan (1982) found that, except in the vicinity of the wall, measurements of longitudinal and radial intensity are similar and also, they remain higher than the corresponding single-phase values. They concluded that the flow remains isotropic and, that bubble turbulence is essentially additive to wall turbulence.

Sim and Lahey (1986) and more recently Lopez de Bertodano et al. (1994) performed experiments in water–air bubble flow in conduits of triangular cross section, aiming at obtaining information regarding the three dimensional character of the flow. Their results

Table 1
Experiments in bubbly flows

Flow type	Work	Test section	Void fraction	Bubble diameter	Water velocity
Pipe flow	Serizawa (1974) and Serizawa et al. (1975)	$\varnothing$60 mm, L = 2.10 m	5–70%	4 mm	0.3–1.03 m/s
	Nakoryakov et al. (1981)	$\varnothing$86 mm, L = 6.5 m	50–80%	Bubble to slug	0.22–2.05 m/s
	Theofanous and Sullivan (1982)	$\varnothing$57 mm	3–20%	3–4 mm	0.23–0.62 m/s
	Michiyoshi and Serizawa (1986)	$\varnothing$60 mm, L = 2.15 m	4–27%	3 mm	0.45–0.77
	Wang et al. (1987)	$\varnothing$57 mm	10–50%	Bubble to slug	0.43–0.94 m/s
	Liu (1997)	$\varnothing$57 mm, L = 8 m	3–28%	1–20 mm	0.5–3.0 m/s
Triangular conduit	Sim and Lahey (1986)	l = 91 cm, base 50.8 mm, height 98.4 mm	66–90%		0.65–1.0 m/s
	Lopez de Bertodano et al. (1994)	$L = 70D$, base 50.8 mm, height 100 mm	10–35%		0.5–1.0 m/s
Boundary layer	Moursali et al. (1995), Marie et al. (1997)	$2.5 \times 0.4 \times 0.4$ m^3	0–55%	3.5–6.0 mm	< 1.5 m/s
Grid turbulence	Lance and Bataille (1982, 1991) and Marie (1983)	$2 \times 0.45 \times 0.45$ mm^3, M = 40 mm, rods 8 mm	0–5%	5 mm	< 1.2 m/s
	Present work	$1.2 \times 0.3 \times 0.3$ mm^3, M = 30 mm, rods 5 mm	0–5%	3 mm	0.25 m/s

indicate pronounced lateral separation and tendency of the dispersed phase to concentrate in areas far from the walls.

Recently Moursali et al. (1995) and Marie et al. (1997) provided information on the development of the boundary layer in a bubbly flow. They found significant migration of the bubbles towards the wall and proposed a modified law of the wall for bubbly flows. Moreover they found that longitudinal turbulence is increased by two mechanisms namely, a modification of the wall production and the creation of pseudo turbulence in the external layer.

More pertinent to the present work are the experiments of Lance and Bataille (1982, 1991) and Marie (1983) on water–air bubble grid turbulence, performed in a facility similar to the one used in the present experiments. Their measurements were obtained mostly at the centre of the test section and 'the underlying idea of their measurements was to simulate as closely as possible the highly idealised situation of a statistically uniform array of bubbles interacting with an isotropic flow field'. Thus contrary to the present case they chose to perform their experiments under constant velocity conditions. They found the existence of two regions, namely, one for low void fraction, where hydrodynamic interactions between bubbles are negligible, and a second one for high void fraction, in which due to their mutual interaction the bubbles transfer a significant amount of kinetic energy to the flow. The measured values of skewness and flatness factors indicate significant departure from normal probability distribution, however, on the basis of measurements of turbulence intensity and Reynolds stresses they concluded, that the structure of turbulence remains isotropic, and that bubble turbulence is additive to grid turbulence. The autocorrelation measurements presented in their work indicate a decrease in turbulent scales with increasing void fraction to a final pattern which remains unaltered for further increase of void fraction. The measured power spectra in this work exhibit a $-\frac{8}{3}$ power form.

The aim of the present study is to provide information about the void distribution and the

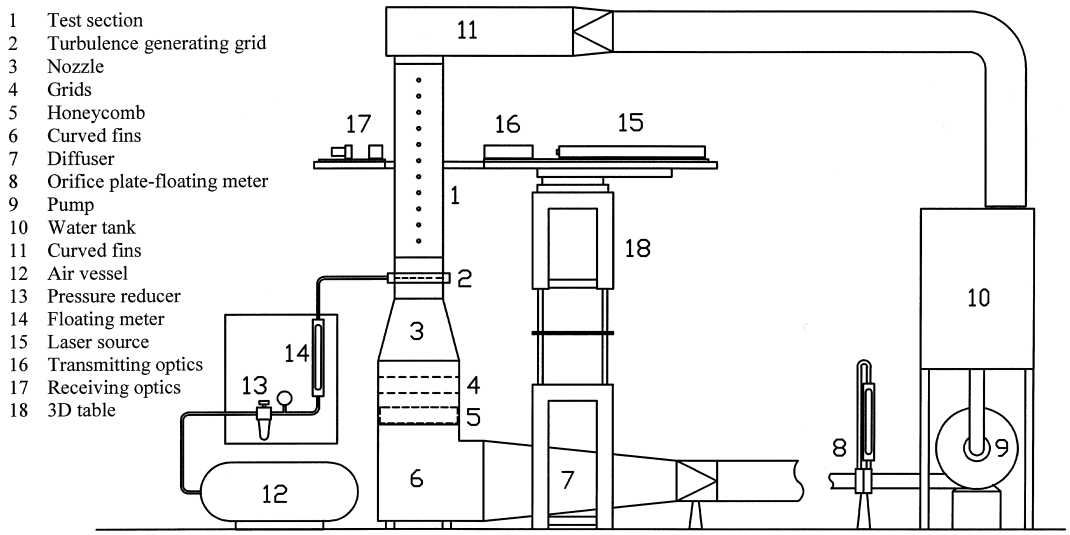

Fig. 1. Side view of the experimental facility.

turbulence structure due to the interaction of the dispersed phase with evolving grid turbulence as it was allowed to be exposed to the influence of the channel's constraining walls by maintaining a constant water volumetric flow rate. The corresponding single-phase Reynolds number was low so that the turbulence energy introduced to the flow due to buoyancy was significant as compared to the single-phase flow turbulence. The presented experiments are conceptually different to those performed by Lance and Bataille (1982, 1991) differing to their respective scope and involving different scales and energy budget. Therefore the two studies are rather complimentary than comparable to each other.

2. Experimental apparatus and equipment

The experiments have been conducted in the two-phase water channel operating in the Laboratory of Thermodynamics shown in Fig. 1. The test section is 1200 mm long with a square cross section of width, $B = 300$ mm. It is positioned vertically with the mean flow of water directed upwards. Two facing walls of the test section are constructed from plexiglas allowing Laser Doppler Velocimetry (LDV), and visualisation techniques to be used. Probes can be inserted in the flow through openings at 100 mm intervals on the third wall.

The grid placed at the test section entrance forms a biplane square, consisting of copper tubes with outside diameter of 5 mm, crossed at mesh spacing $M = 30$ mm. It is also used for the injection of the bubbles, through hypodermic needles of inside diameter 0.2 mm, located at the copper tube crossings. The volumetric air flow rate is regulated by a pressure reducer and measured with a variable area flowmeter.

The water velocity field is monitored with a dual beam forward scatter LDV system, the transmitting and the receiving optics of which were mounted on a carrying table capable of moving in three directions. This measuring technique has been selected because of its non intrusive character. A summary of the LDV setup is presented in Table 2.

Table 2
LDV system summary

Laser source	He–Ne 15 mW Spectra physics
Laser wavelength	632.8 nm
Beam diameter (e^{-2} intensity)	1.1 mm
Beam separation	50 mm
Focal length of lenses	250 mm
Frequency shifter	Single Bragg cell (TSI)
Receiving optics azimuth	5°
Elevation angle	0°
Pinhole	100 μm
Receiving aperture	20 mm
Photodetector	Photomultiplier TSI
Signal processor	Counter TSI 1980-B
Data acquisition	Analog output of counter, 14 bit A/D Converter, maximum sampling frequency 16 kHz, PC-86 computer

Data points of velocity departing more than three times the variance from the mean value were rejected considered as noise (Marie and Lance, 1984). For every measuring position an ensemble of up to 10 data samples was collected, corresponding to a total recording time of at least 5 min. Each signal sample consisted of 20,000 digitised values, the sampling rate being 100 Hz. Although the validity of high frequency spectra based on LDV measurements is questionable, the data rate, the continuity of the signal as well as the spectra estimation technique (described in Section 3) allowed the estimation of power spectra with a wide range of frequencies at the centre of the cross section. These spectra were obtained from ensembles of 20 data samples each consisting of 20,000 digitised values sampled at 2 kHz, thus containing information covering frequencies up to 1 kHz.

Local void fraction measurements were conducted with an Optoflow fiber optics probe as well as with hot film anemometry by using a TSI 1050 anemometer with a cylindrical probe (TSI 1210-60 W).

Bubble measurements were conducted with double-exposure photography (Mahalingam et al., 1976). A double light source, flashing with controlled time lag, was directed through the side wall openings producing a vertical plane light beam twice. A photographic camera, placed in front of the plexiglas window, was taking two successive pictures of the bubble field on the same plate. Bubble diameters and bubble velocities were calculated from the enlargements. It was found, that bubble mean diameter was 3 mm, while bubble mean slip velocity, for low void fraction, was approximately 250 mm/s.

The presently existing methodology on the accuracy of two-phase flow measurements is not sufficiently developed to allow a reasonable error estimation in many cases. This limitation is reflected in the absence of extensive accuracy discussion in the majority of the reported experimental work. Topics such as the interaction of the bubbles with the probe, the discrimination of the phases and the removal of the bubble signal from the water velocity signal, are seldom discussed in relation to accuracy. In the present experiments the accuracy of the void fraction measurements is of the order of 5% in the case of the optical probe (Moursali et al., 1995) and by comparison has been estimated to be 8% in the case of the hot-film probe. The effect of the phase discrimination procedure in the estimation of mean velocity has been tested. Mean velocity values were less than 3% affected by changing the percentage of the variance used as the limit of the velocity distribution. Taking this into account as well as the LDV accuracy and the sample length it is reasonable to accept an overall precision of better than 5% for the estimation of mean velocity, although higher order moments of the velocity are expected to be less accurate.

3. Experimental techniques

The interpretation of the measured signals revealed significant problems demanding to be addressed in two-phase flow measurements. The techniques developed to overcome these problems are presented in the following.

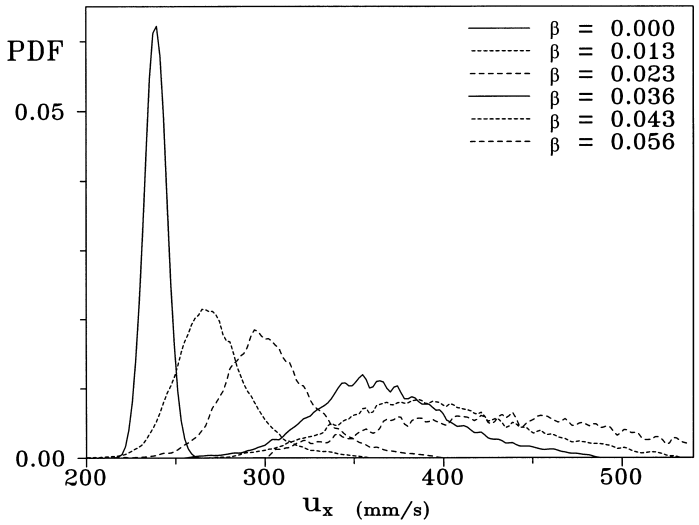

Fig. 2. Probability density function of longitudinal velocity at the centre of the test section.

3.1. Discrimination of phases in LDV measurements

The discrimination of phases is of primary importance in two-phase flow measurements. The issue becomes very important with LDV measurements since in dispersed two-phase flow velocity measurements, both phases may contribute to the recorded signal. Moreover in dense flows significant dropout may occur due to the blockage of the optical path.

During the experiments the quality of the signal from the counter was very satisfactory as it presented good continuity and data rate on the oscilloscope. The probability distribution function of the velocity shown in Fig. 2 presented only one peak in support to the view that no bubble velocities were measured. At the time those measurements were performed it was considered that amplitude discrimination had been achieved. However, later Panidis and

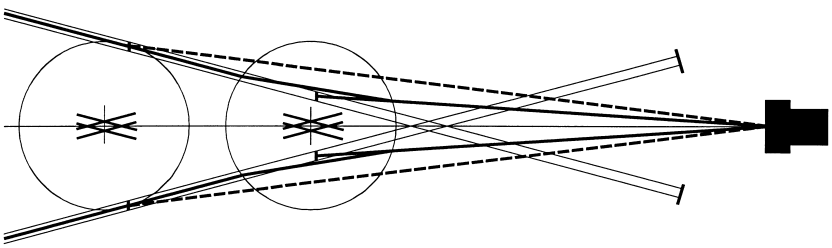

Fig. 3. Location of scattering particle for reflection and first order refraction (thin lines: laser beams, heavy lines: ray tracing dashed for reflection, solid for refraction, vertical line segments on the beams represent apparent points of transmission).

Sommerfeld (1997), introducing the Locus of Centre (LoC) method for LDV analysis, proved that with the optical setup used it was not possible to obtain velocity measurements from the large bubbles of the flow under investigation. The reasons are briefly discussed for clarity in the following while a complete analysis of the problem can be found in the above mentioned reference.

As shown in Fig. 3 large spherical particles are transmitting heterodyned signals to the photodetector while being at different locations for each mode of transmission (i.e. reflection, simple refraction etc.) and given that the photodetector is viewing the corresponding apparent points of transmission on the beams. The analysis is based on the study of the properties of the Locus of Centres of the beams that is the locus where the centre of a particle should be, in order to transmit light to the photodetector from each beam. The beams' LoC crossing defines the LoC control volume and corresponding apparent transmission points on the beams can be determined. The displacement of the LoC control volume relative to the beam crossing is proportional to the particle size while the direction and the constant of proportionality of the displacement are functions of the beams' orientation, the location of the photodetector and the mode of transmission.

For the optical setup used the position of the beams and the corresponding beams' LoC for reflection and first order refraction are shown in Fig. 4, for bubbles of 2 mm diameter (the laser beams are propagating on the zx plane towards positive z). The vertical lines on the beams indicate the apparent transmission points which must be viewed by the photodetector in order to get heterodyned Doppler bursts. Since during the present experiments the photodetector was focused on the beam crossing and the bubbles in the flow were about 3 mm in diameter, it becomes clear that no bubble velocity signals were processed.

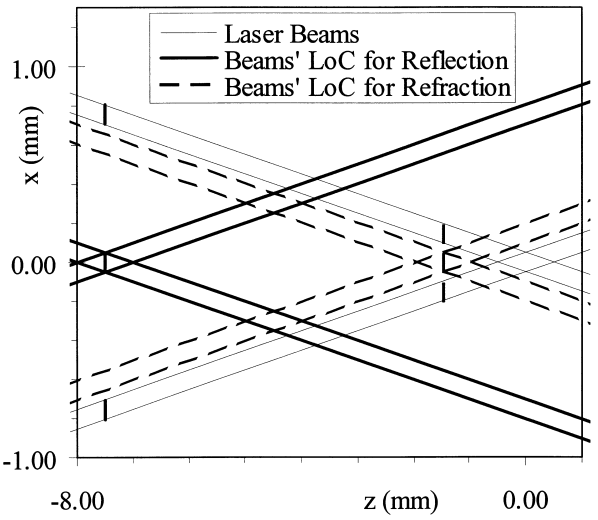

Fig. 4. Location of reflection and refraction LoC control volumes for the optical setup used.

3.2. Void fraction measurements with hot film

The problem of identifying the passage of a gas bubble in the continuous signal generated by a hot film sensor immersed in a liquid–gas flow, has been addressed by several investigators. Serizawa (1974), Wang et al. (1987) developed 'bubble signature' pattern methods. Lance and Bataille (1982, 1991) employed the quantity $(\delta u_L^2/\delta t)^2$ used in turbulent intermittency experiments, while Marie et al. (1997) used a thresholding technique applied to the signal's time derivative. In the present experiments an algorithm has been developed, similar to the one suggested by Wang et al. (1987) and Marie et al. (1997). The detection of the bubble's passage is accomplished by using the gradient $\Delta E/\Delta t$, where E is the hot film signal. Entrance of the bubble is marked by an increase of the gradient's value above a preset level, while its exit by an abrupt change of the signal to the level corresponding to liquid velocity measurements. The above mentioned algorithm is used for the construction of a phase discriminating function, χ, with value one indicating that the sensor is completely immersed in the continuous phase at the time of the measurement and zero otherwise.

If the sensor was infinitesimally small the local void fraction, ε_G, would be the time fraction that void is present on the sensor i.e.,

$$\varepsilon_G \equiv \lim_{T\to\infty} \frac{t_p}{T} = \frac{\sum_{i=1}^{N}(1-\chi_i)}{N} = 1-\bar{\chi} \tag{1}$$

where t_p the total time that void is present at the measuring point, T the total measuring time, N the number of samples and $\bar{\chi}$ the mean value of χ_i $(i = 1,2,\ldots,N)$.

Since the sensor has finite physical dimensions and it is discriminating void as soon as any part of it is in contact with a bubble it is sensing the void for larger time fractions, ε_s, than the infinitesimal one. Panidis (1996) has calculated the correction factor, c,

$$c = \frac{\varepsilon_G}{\varepsilon_s} = \frac{\varepsilon_G}{\lim_{T\to\infty} \frac{t_s}{T}} = \frac{\varepsilon_G}{1-\bar{\chi}} \tag{2}$$

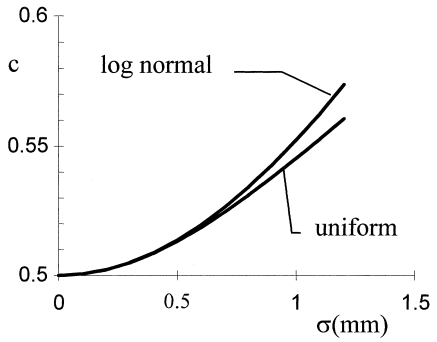

Fig. 5. Correction factor c as a function of the particle size distribution variance.

Table 3
The correction factor c for simple diameter distributions

Distribution	$p(D)$	c
Constant $D = d$	$\delta(D-d)$ (Dirac delta)	$\frac{2d}{2d+3l}$
Uniform in $[(d-\varepsilon),(d+\varepsilon)]$, $\mu = d$, $\sigma^2 = \frac{\varepsilon^2}{3}$	$1/(2\varepsilon)$ for $d-\varepsilon < d+\varepsilon$, 0 otherwise	$\frac{2d}{2d+\frac{3d^2+\varepsilon^2}{d^2+\varepsilon^2}l}$
Logarithmic normal $\mu = \exp(\lambda + \frac{1}{2}\zeta)$, $\sigma^2 = \mu^2(\exp(\zeta^2)-1)$	$\frac{1}{\sqrt{2\pi\zeta}D}\exp(-\frac{1}{2}(\frac{\ln D-\lambda}{\zeta})^2)$	$\frac{\exp\left(3\lambda+\frac{(3\zeta)^2}{2}\right)}{\exp\left(3\lambda+\frac{(3\zeta)^2}{2}\right)+\frac{3l}{2}\exp\left(2\lambda+\frac{(2\zeta)^2}{2}\right)}$

which should be used to calculate the void fraction from the time fraction that the sensor is in contact or covered by a bubble (t_s is the total time that the sensor is in contact with a bubble). The derivation assumes non deformable spherical bubbles. It is further supposed that all the bubbles are pierced as they are moving with high velocities against the probe prong tips. The void fraction is considered constant in the vicinity of the probe and low enough to ensure that only one bubble may be in contact with the probe. Monodispersed as well as bubbles following uniform or logarithmic normal size distributions have been considered. The equations giving c as a function of the sensor's length, l, the mean diameter, μ, and the variance, σ, of the bubble size distribution are presented in Table 3. The values of c for mean bubble diameter $d = 3$ mm and sensor length $l = 2$ mm are given as a function of the distribution variance in Fig. 5. In the present work the value of $c = 0.5$ corresponding to the monodispersed case has been used for the calculation of the void fraction.

Although the measurement of local void fraction with a cylindrical hot film probe has been questioned by several investigators (Serizawa et al., 1984; Wang et al., 1987; Farrar and Bruun, 1989) this technique was the only available at the time the main body of the presented data was acquired. Later, measurements of local void fraction with an optical probe produced results consistent with those of the hot film technique, both of which will be presented in Section 4.

3.3. Correlation and spectra of two-phase flow signals

In computing statistical moments, and autocorrelations in two-phase flows the problem of the intermittent character of the liquid phase velocity signal arises. To evaluate the Fourier transform of such a signal function, analytic continuity should be established. Gherson and Lykoudis (1984) overcame this difficulty by simply removing the part of the signal corresponding to the dispersed phase, and patching the velocity segments together. This technique clearly alters the temporal dependency of velocities. Lance and Bataille (1982, 1991), applied rectangular and Laplace–Gauss smoothing windows to a hot-film signal. The rectangular window process assumes, that in the area occupied by the bubbles the water velocity is equal to the mean velocity of the flow and correlates this velocity, which is hypothetical, with the validated part of the velocity signal thus introducing high frequencies in the spectral estimator. In fact the water velocity is not defined in the segments corresponding to the presence of the bubbles. In regard to the use of other smoothing windows, as for instance the mentioned Laplace–Gauss, it appears that, in general they introduce non-existing eddy representation in the autocorrelation function. This is because their application to the hot film signal corresponding to bubble passage, meaningless as far as continuous phase velocity is concerned, results to non-zero misleading contribution to the signal representing this velocity. It should be added that, even in the case of successive application of a rectangular and a smoothing window, a process which might present some advantage, the limitations inherent to the rectangular window application are not alleviated.

In the present work a different approach has been adopted to overcome the above mentioned difficulties (Panidis, 1995). The methodology is rather simple consisting of the following steps: (i) start with a complete digitised signal, lets say a single-phase flow signal, (ii) randomly eliminate a number of the digitised values, (iii) find an estimator for the

autocorrelation of the defective remaining signal which will give the same result as the original signal's autocorrelation and (iv) apply this estimator to any signal with missing values such as due to bubble presence or poor data rate due to dense flow etc. Subsequently, the power spectrum can be derived from the autocorrelation function as expressed above by applying Fourier transform.

Suppose a digitally sampled velocity signal representative of a single-phase turbulent flow, u_i ($i = 1,\ldots,N$), sampled at time intervals $\Delta\tau$. Denoting with u_i' the fluctuations of the velocity about the mean value, the autocorrelation at time lag $n\Delta\tau$ (n integer) can be estimated as

$$B_{jj}(n\Delta\tau) = \lim_{N\to\infty} \frac{\sum_{i=1}^{N-n} u_i' u_{i+n}'}{N-n} \tag{3}$$

That is, the autocorrelation is the mean value of the corresponding products $u_i'u_{i+n}'$, $i = 1,2,\ldots,N$, which follow a certain PDF. If some of these products are eliminated using a random function m_i, $i = 1,2,\ldots,N$, having the value 1 for the remaining products and 0 for those to be eliminated, the PDF will not be altered and the mean value can now be estimated by

$$B_{jj}(n\Delta\tau) = \lim_{N\to\infty} \frac{\sum_{i=1}^{N-n} u_i' u_{i+n}' m_i}{\sum_{i=1}^{N-n} m_i} \tag{4}$$

Thus for any signal u_i and a characteristic function χ_i ($i = 1,2,\ldots,N$), having the value one for the validated samples and zero for the rejected ones, the autocorrelation can be estimated by Eq. (4), setting $m_i = \chi_i\chi_{i+n}$.

In order to apply this technique to two-phase flow signals the statistics of χ_i should be considered. If χ_i is only a phase discriminating function indicating the presence or absence of a phase in the measuring volume no problem arises. However if χ_i takes also into account sample values that are missing or are rejected due to other reasons, it is necessary to ascertain that no biased effects are introduced. For example, in LDV measurements when some values are missing due to beam interruption by the bubbles, it should be ascertained that there is no systematic hiding of phenomena due to specific bubble structures. Otherwise all the statistics of the velocity field are expected to be biased. Equally important are the statistics of the summation $\sum(\chi_i\chi_{i+n})$ which is the number of validated products to be used for the estimation of the autocorrelation function. If this number of products is not the same (within statistical uncertainty limits) for all the time lags $n\Delta\tau$, then the autocorrelation function values are not equivalent resulting to a biased energy distribution over the flow scales as described by the power spectrum. These topics will be further discussed in the next section in which a method to control their effect will also be presented.

In conclusion, the present technique of introducing an indirect analytic continuity applied in the computation of all the statistical quantities, essentially presumes that the void portion of

the signal has been filled with segments having the same statistical properties as those of the water velocity signal. This assumption does not require that the missing part of the velocity signal could actually be reconstructed. It differs from the rectangular window technique and hence from subsequently applied smoothing windows, since for the latter the denominator remains $(N-n)$ thus departing statistically from the continuous signal autocorrelation value as the number of missing products increases with increasing void fraction.

To check the validity of the employed technique and also to compare it with that of the rectangular window, the following computational experiment was performed. A continuous signal representing turbulence motion was devised consisting of 2×10^5 digitised values sampled at 2 kHz. In this signal a characteristic function χ_i was applied in which patches of $\chi_i=0$ corresponding to the presence of bubbles were created randomly, with arrival times following a beta distribution and lengths following normal distribution. Employing the described process, four cases were constructed of signals corresponding to two-phase turbulence of 2, 5, 10 and 15% void fraction, respectively. The four signals were subsequently processed by employing the two mentioned methods and the obtained power spectra were compared to that corresponding to the continuous signal as shown in Fig. 6. In this figure, solid line represents the spectrum obtained from the continuous signal on which all four cases of different void fraction processed with that adopted in the present experiments method fall. Contrary, in the case of the rectangular window technique the obtained spectra appear to depart increasingly with void fraction at low frequencies from that corresponding to the continuous signal.

3.4. Bubble structure

The detection of organised bubble structures is very important for the study of the

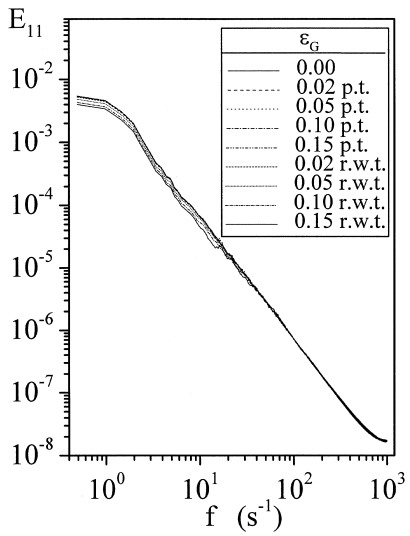

Fig. 6. Comparison of spectra derived with the presented technique and the rectangular window technique.

properties of dispersed two phase flows. Moreover as mentioned in the preceding section it is significant for the correct estimation of the statistics of the flow. For this purpose the autocorrelation coefficient of bubble presence, R_b, was used, defined as the probability that the measuring point being at time t in the dispersed phase is also in the same phase at time $t + n\Delta\tau$ ($n = 0,1,2,\ldots$):

$$R_b(n\Delta\tau) = P\big((\chi_{i=n} = 0)/(\chi_i = 0)\big) = \frac{P(\chi_{i+n} = 0 \text{ and } \chi_i = 0)}{P(\chi_i = 0)} = \lim_{N\to\infty} \frac{\sum_{i=1}^{N-n} \frac{(1-\chi_i)(1-\chi_{i+n})}{N-n}}{\varepsilon_G} \tag{5}$$

The coefficient R_b fluctuates with n between the values 1 and 0 for signals corresponding to a regular succession of bubbles passing the measuring point, while it takes the value of the local void fraction, ε_G, for varying n, in the case of random succession of bubbles corresponding to statistically independent events. If χ_i has been calculated from a hot film signal, taking into account the dimensions of the probe, in the above derivation of R_b, ε_G has to be replaced by $\varepsilon_s = \varepsilon_G/c$ that is,

$$R_b(n\Delta\tau) = \lim_{N\to\infty} \frac{\sum_{i=1}^{N-n}(1-\chi_i)(1-\chi_{i+n})}{(N-n)\frac{\varepsilon_G}{c}} \tag{6}$$

and complete randomness corresponds to the value of R_b equal to ε_s for varying n. It has to be noted that the coefficient R_b is very important for the reliable estimation of the autocorrelation in two-phase flows with the technique discussed in the preceding section. For samples long enough to ensure statistical convergence, R_b is a function of only the ε_s and the summation $\sum(\chi_i\chi_{i+n})$ that is, the number of validated products for the estimation of the autocorrelation function. Simple statistical calculations show that R_b is a very sensitive indicator of the behaviour of $\sum(\chi_i\chi_{i+n})$ and that if it fluctuates randomly close to ε_s for varying n the request of equal importance for the autocorrelation function values is accomplished. Moreover the absence of bubble structures is indicative of the lack of bias introducing beam interruptions in LDV measurements.

4. Experimental results and discussion

The measurements in the present work were obtained at a distance of 900 mm from the turbulence generating grid, equivalent to 30 mesh. Moreover, in all the conducted experiments the water volume rate was maintained constant at a corresponding single-phase Reynolds number, based on mesh length, equal to $Re_M = 8000$. The coordinate system to which the measurements are referred is oriented with the x-axis parallel to the mean flow, the y-axis, along which the longitudinal velocity measurements were conducted, in the direction

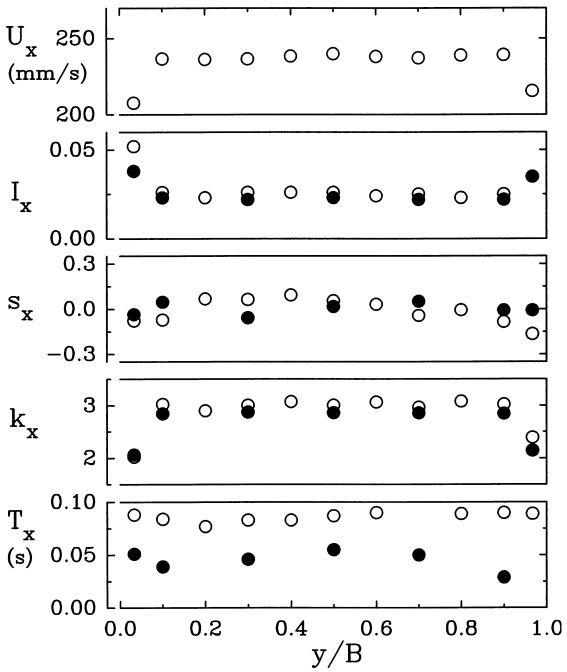

Fig. 7. Measurements of single phase flow (○: longitudinal, ●: transverse components).

perpendicular to the transparent test-section's walls, while the void fraction measurements were conducted along the direction of the z-axis.

4.1. The structure of the single-phase grid turbulence

To check the flow quality in the test section, and also to establish a frame of reference for the evaluation of the influence of the dispersed phase on the structure of grid turbulence, its mean and statistical characteristics were investigated and the obtained results were compared with well established in the literature single-phase grid turbulence measurements (Stewart,

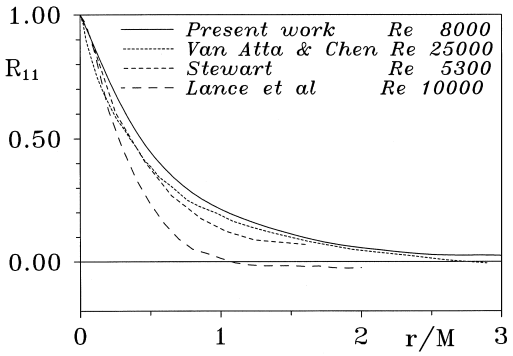

Fig. 8. Single phase flow longitudinal autocorrelation.

1951; van Atta and Chen, 1968, 1969). The measured distributions of mean velocity U_x, and those of statistical quantities such as turbulence intensity I, skewness s, and flatness k, factors, macroscales T, and longitudinal autocorrelation R_{11}, are presented in Figs. 7 and 8. It is observed that these measurements show the existence of a turbulent flow region occupying the central part of the test section, characterised by uniform values of both mean, and statistical parameters. In this part, the level of the turbulence intensity is 2.5% of the mean velocity, and the skewness and flatness factors are approximately zero and three, respectively for both the longitudinal and transverse velocity components. These values correspond to a turbulence field characterised by a Gaussian probability distribution function. Finally, in Fig. 8 the autocorrelation obtained in the present experiments is compared with existing similar measurements. It appears that there is fair agreement especially as far as the integral scales are concerned with corresponding results measured in air by Stewart (1951) and van Atta and Chen (1968), while there is a difference with the measurements of Lance and Bataille (1982) obtained in a water channel similar to the one described in the present work.

In conclusion, the discussed results indicate, that the structure of the grid turbulence in the central part of the channel's test section is nearly isotropic, exhibiting statistical characteristics comparable to those corresponding to well established similar measurements in the literature.

The influence of the dispersed phase on the originally isotropic turbulence flow field is discussed in the following, as inferred from the obtained measurements.

4.2. Mean characteristics of the two-phase turbulence field

Measured profiles of the local void fraction ε_G, along the z-axis are shown in Fig. 9. It can be seen that for low volumetric gas flow rate ratio, β, the presented profiles of ε_G are shifted uniformly to higher values as injection of the dispersed phase is increased, retaining their flat form. For higher gas flow rate the profiles change drastically, developing peaks located approximately at midpoint between the wall and the centre of the channel, while close to the wall the void fraction remains relatively low. As shown in Fig. 10 similar peaks are observed in

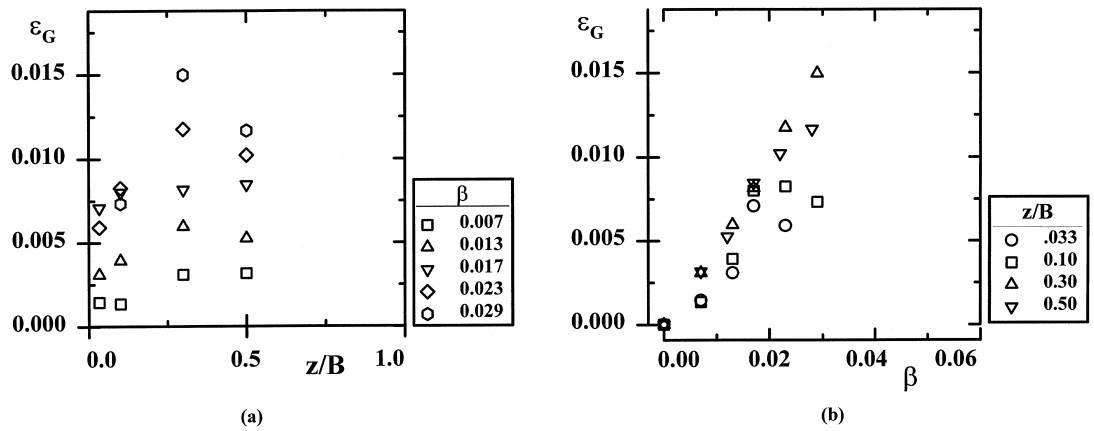

Fig. 9. Evolution of local void fraction.

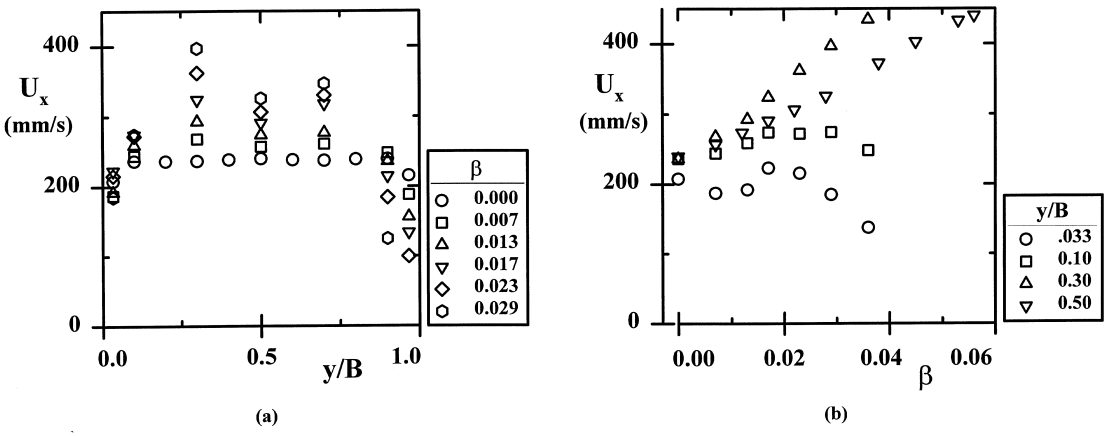

Fig. 10. Evolution of longitudinal mean velocity.

the profiles of the longitudinal mean velocity, U_x, along the y-axis that is, in the direction perpendicular to that of the void fraction profiles. Thus it is plausible to assume that peaks in the channel develop in a peripheral pattern.

In order to investigate the origin of this effect that is, the possibility to originate from the presence of particular inlet conditions dominating the entrance of the test section, the upward development of void distribution in the channel has been monitored with an optical probe. Accordingly measurements of the local void fraction at several distances from the grid are presented in Fig. 11. It should be noted that due to changes in the channel's operational conditions these measurements were conducted at a Reynolds number, based on the grid mesh, equal to 7000. Moreover the values measured close to the wall might be overestimated due to bubble sliding from the wall to the probe tip. As these measurements show, very close to the grid the void distribution is dictated by the bubble injection pattern as clearly indicated by the peak values of void fraction attained at close distance above the injector locations. The lower void fraction values at the centre of the channel shown in Fig. 11 at $2.3M$ is due to the sensitivity exhibited by the sensor at this low distance to small displacements in its positioning as related to the injector. Starting at the height of 7 mesh distances, M, a drastic change develops in the void fraction distribution with the elimination of the peaks corresponding to the second injector from the wall. This development continues upwards terminating to a final distribution of void fraction consisting of two distinct areas located at the central part and close to the wall of the channel, respectively. This two-peak void fraction distribution persists farther up to $27M$ where the distribution is characterised by only one peak located between the centre and the wall of the channel, which is preserved thereafter. On the basis of the discussed evidence it can be concluded that the observed peak development is the result of processes inherent to the nature of the investigated two-phase flow pattern rather than the outcome of inlet conditions of the particular configuration.

Peak development in the void fraction distribution close to the wall has been reported among several other investigators by Serizawa et al. (1975), Theofanous and Sullivan (1982)

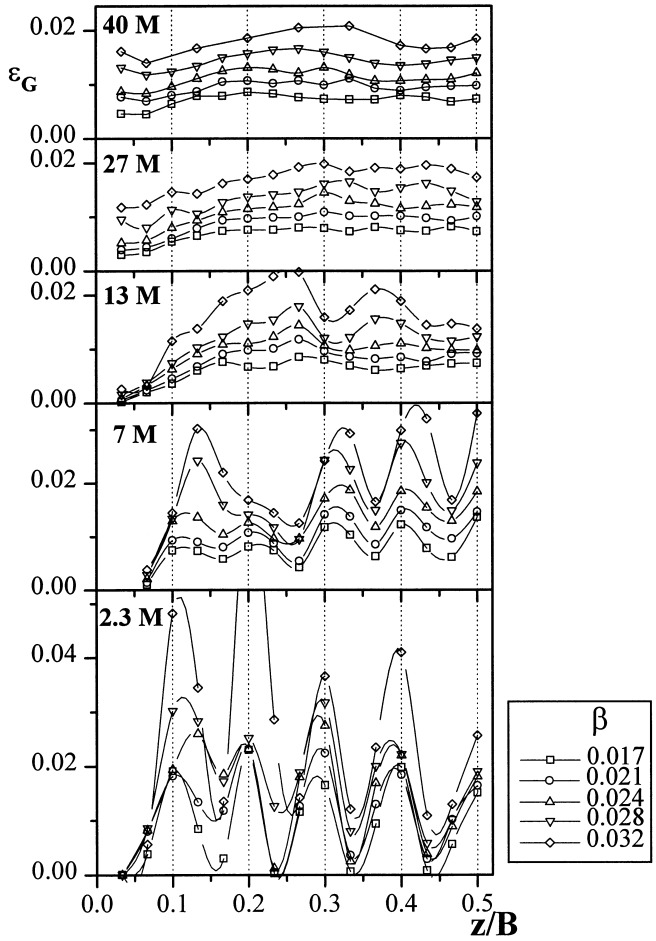

Fig. 11. Development of the local void fraction profile along the channel.

and Wang et al. (1987) in upward pipe flow and more recently by Marie et al. (1997) who investigated the void peak development in a bubbly boundary layer.

Following Marie et al. (1997) most of the observed void peaking phenomena could be attributed to the deceleration of the bubbles at the surface of the wall and to the deflection of a significant number of bubbles towards the walls. These phenomena, not possible to be monitored in the present experiments, are observed close to the wall, at distances comparable to the bubble diameter.

The void peaking measured in the present experiments is comparable to that observed by Sim and Lahey (1986), in triangular conduits and in air–solid particle two-phase flow in horizontal pipes by Tsuji and Morikawa (1982). Secondary peaks indicative of the same underlying phenomena are observed in void fraction measurements at low velocities of Michiyoshi and Serizawa (1986) and Wang et al. (1987) in pipe flow, as well as in those of Moursali et al. (1995) and Marie et al. (1997) in boundary layer flow.

Contrary to the wall peaking reported in the previous experiments, the void peak

development in the present work is accompanied by a matching axial velocity distribution. The observed phenomenon might be the result of the lift force due to the interaction of the particle with the local shear as in the Segre and Silberberg (1962) effect according to which "a rigid sphere transported along in a Poiseuille flow through a tube, is subject to radial forces which tend to carry it to a certain equilibrium position at about 0.6 tube radii from the axis". The direction of the lift force in bubbly flows is sensitive to the bubble deformation and the Reynolds number (Esmaeeli and Tryggvason, 1996; Tomiyama et al., 1995). The resulting void distribution is the outcome of equilibrium attained between interdependent forces such as the restricting effect of the walls, the lift, the drag and the buoyancy force and thus it is very difficult to be predicted. Another possible mechanism associated with the presence of large eddies may also be responsible for the bubble migration. This mechanism suggested by one of the referees has been adopted and discussed by the authors as a possible one. The velocity distribution and the high level of turbulence close to the wall are consistent with the presence of large eddies developing in the channel. In this case the void distribution is possibly affected by a bubble entrainment and capture process into these structures. In the present case the phenomenon is probably dominated by the low water velocity and the relatively large channel cross section and is representative of the stage of flow development. The topic is very interesting although complicated and it is closely related to the question of attaining a final state of self preservation of the flow structure, deserving further experimental investigation. It has been also the subject of investigation for simpler flows with the aid of Direct Numerical Simulation (DNS) (see, for example, Ervin and Tryggvason, 1997; Loth et al., 1997; Kim et al., 1993).

The high concentration of the bubbles at the location of void peak results in a significant increase of the water velocity in this area due to buoyancy and the interfacial drag leading to further rearrangement of the velocity distribution due to continuity.

In the measured mean velocity distribution shown in Fig. 10 peak values as high as almost twice the superficial mean velocity are observed. To verify the validity of the obtained high peak velocity values, the volumetric flow rate estimated from the measured velocity, taking into consideration the local void fraction distribution, was compared with the corresponding directly measured flow rate. The estimated and measured flow rate values were found in good agreement departing less than 4%.

The effect of the dispersed phase on the flow characteristics can be further investigated by considering their dependence on the void fraction at different locations. This information for the local void fraction, ε_G, and the mean velocity U_x, is presented in Figs. 9(b) and 10(b), respectively. Two distinct effects can be clearly identified in these diagrams. First, the development of two regions corresponding to low and high gas flow rate ratio values is evident. It appears, that at low gas flow rate ratio a small increase in its value produces an increase of the local void fraction distribution characterised by a uniform rate over a cross section. Subsequently, its further increase above a critical value of approximately 0.02, results in a substantial decrease of local void fraction near the wall, therefore the appearance of the two distinct spatial regions in which the effect of the dispersed phase is not the same. As shown in Fig. 10 there is a direct effect of the void fraction distribution on the corresponding mean velocity profile which exhibits similar behaviour.

In conclusion as an assessment of the overall effect of the dispersed phase on the mean flow

characteristics it can be stated, that the bubble motion establishes in the central part of the channel a free turbulence flow pattern, while a boundary layer of considerable thickness develops near the walls as a result of bubble–wall interaction.

4.3. Statistical characteristics of the two-phase turbulence field

The observed changes in the measured distributions of statistical quantities such as turbulence intensity, I, skewness, s, and flatness, k, as well as the corresponding alterations in the turbulence structure are subsequently discussed.

It appears interesting to compare the measured turbulence intensities of the longitudinal, and transverse velocity components. As shown in Fig. 12, the existence of low, and high gas flow rate regions is clearly evident in the measurements of the longitudinal turbulence intensity, I_x, although the identified effect of the dispersed phase on the spatial distribution is less pronounced. In general the obtained distributions of the intensity component I_x, exhibit a nearly uniform increase with gas flow rate at the central part for low values of gas flow rate ratio, maintaining a nearly flat profile with a higher rate of intensity increase occurring near the walls. For higher gas flow rate values this turbulence intensity component, increases at a reduced rate, while its spatial distribution is characterised by a less extended flat part. A different behaviour is observed in the transverse component, I_z, measured distributions. After a jump corresponding to the change from single-phase flow to low gas flow rate ratio two-phase flow, no significant changes occur with increasing gas flow rates (Figs. 13 and 14). The central part of the transverse intensity, I_z, distributions remains flat, while for low gas flow rates little variation is observed near the walls. However, for higher gas flow rates the intensity near the wall increases. The described behaviour characterises the transverse intensity components across the test section in both the y-, and z-directions.

The observed differences in the intensity component distributions as discussed above, clearly indicate a preferential increase in the longitudinal component, to occur at the central part of

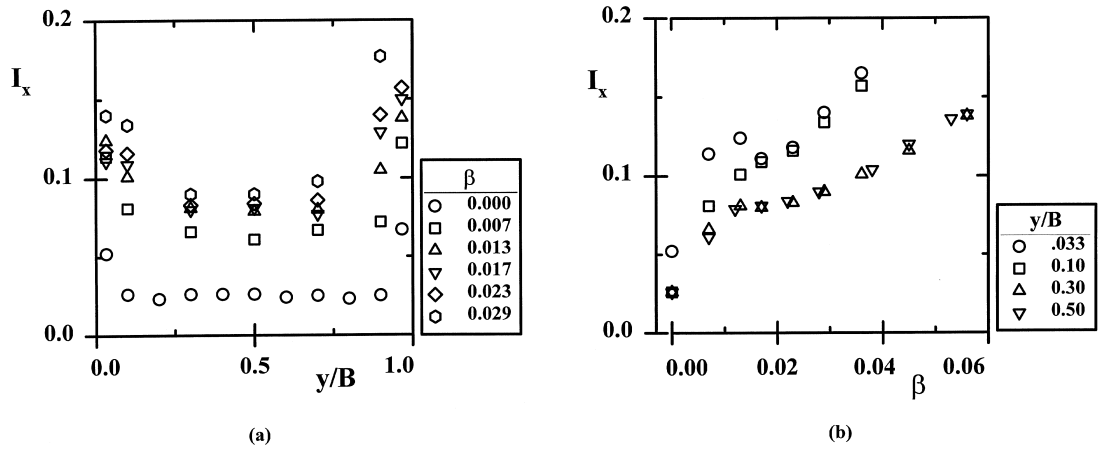

Fig. 12. Evolution of longitudinal turbulence intensity.

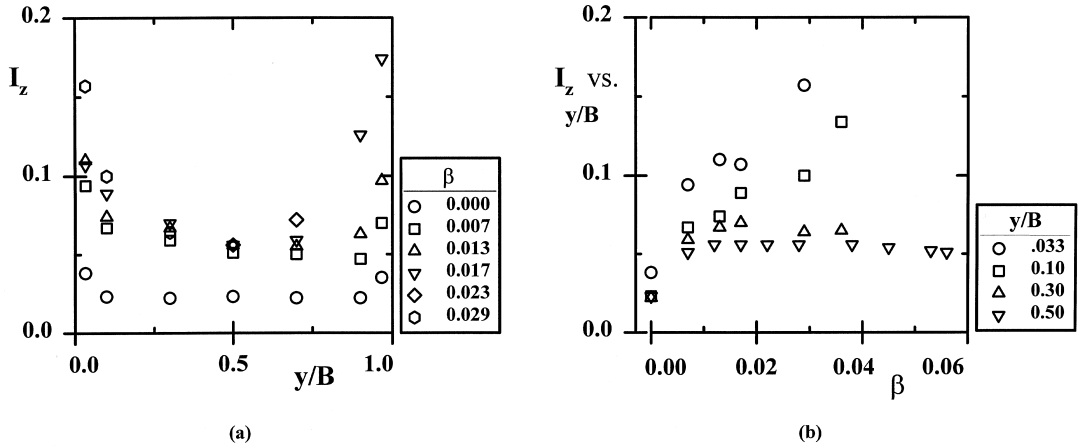

Fig. 13. Evolution of transverse turbulence intensity along y-axis.

the cross section with increasing gas flow rate. An explanation of the observed preferential strengthening of the axial turbulent intensity component is offered next. The range of the axial velocity fluctuations in the corresponding probability distribution function, on which the level of the intensity in this direction depends, is determined by the lower limit of the single-phase velocity and the higher limit of terminal bubble velocity as imposed by interfacial drag. As the gas flow rate increases the bubble terminal velocity increases due to the higher water mean velocities and its interrelating effect with the interfacial drag. This results in a broadening of the corresponding PDF responsible for the observed increase in the axial velocity intensity. Regarding transverse component fluctuations their increase depends on bubble wake turbulence which after the occurrence of the mentioned jump from single-phase due to their presence, remains proportional to the axial mean velocity with minor effect on transverse intensities. Furthermore, the bubble interaction with the wall boundary layers is responsible for the observed increase of both turbulence intensity components close to the walls. Finally it appears

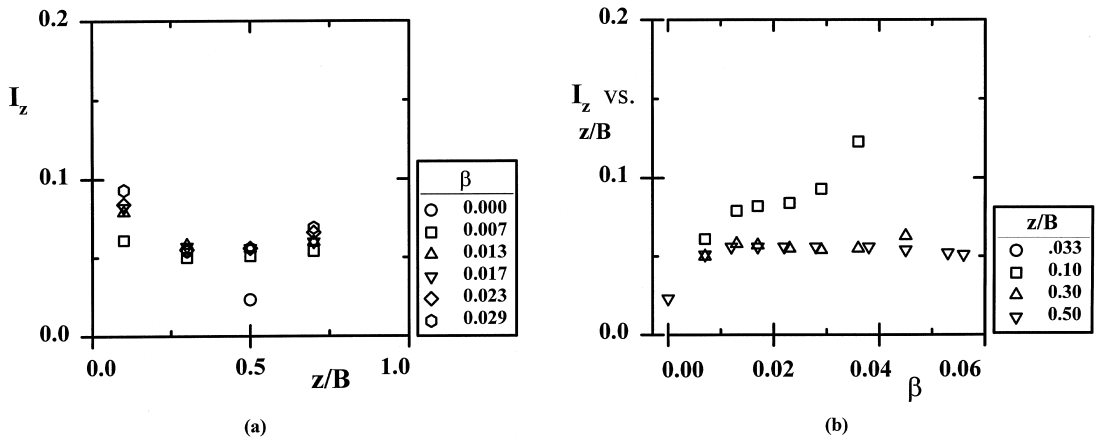

Fig. 14. Evolution of transverse turbulence intensity along z-axis.

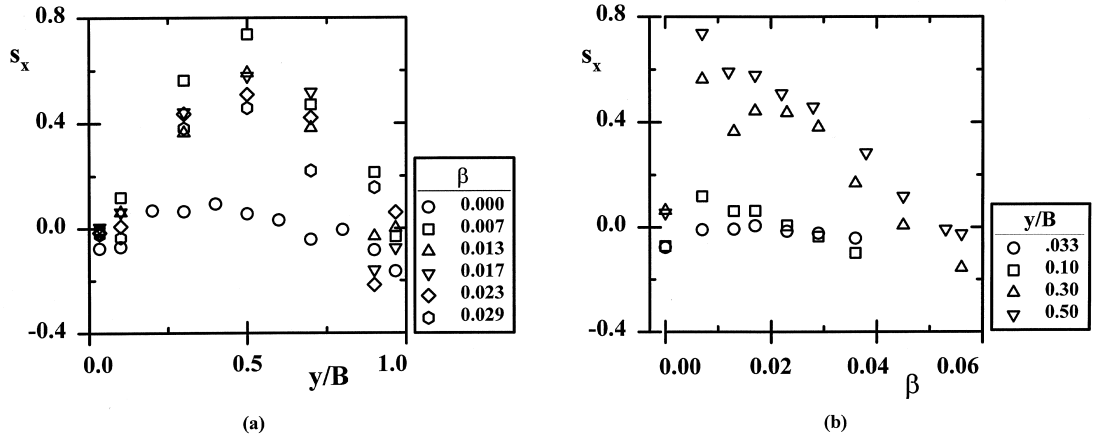

Fig. 15. Evolution of longitudinal skewness factor.

that, the discussed unequal change observed in the longitudinal and transverse intensity components causes the previously nearly isotropic turbulence field to depart progressively from isotropy with increasing presence of the dispersed phase.

Inspection of the skewness and flatness measurements in the longitudinal direction, s_x, and, k_x, respectively, shown in Figs. 15 and 16, offer complementary information regarding the effect of the dispersed phase on the turbulent flow field of the continuous phase.

First, significant changes occur in the turbulence structure, starting with the introduction of bubbles as evidenced by the abrupt increase of the two factors, measured at the minimum value (0.007) of the gas flow rate ratio. It should be noted that, no significant departure from isotropy is evident in the measured turbulent intensity components at this low gas flow rate indicating that, those factors appear more sensitive in recording departure from isotropy. Subsequent increase of the gas flow rate ratio beyond the mentioned value, results in a progressive return of the skewness and flatness towards their values corresponding to a

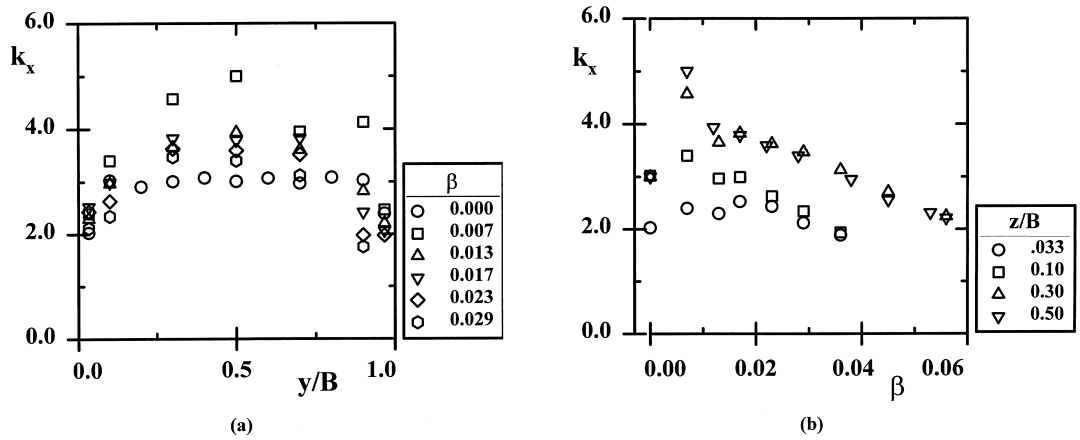

Fig. 16. Evolution of longitudinal flatness factor.

Gaussian distribution. An interpretation of the discussed observations, connecting them to corresponding changes in the turbulence field, can be sought by considering the views of Townsend (1976) on the physical meaning of skewness and flatness in ordinary turbulence in combination with those expressed by Tsuji and Morikawa (1982) for particle laden flows. Briefly, according to Townsend, high values of skewness and increased values of flatness as related to those corresponding to isotropy, are respectively indicative of turbulence energy convection and the presence of inhomogeneities in the turbulence field. Corresponding changes in two phase flows should be attributed, according to Tsuji and Morikawa, to energy exchange between the turbulent main flow field and those formed around and within the wakes of the moving particles caused by existing velocity differences between those fields. The final result of this process is the introduction of an asymmetry in the flow velocity probability distribution function.

In the case of water–air bubble flow under study, the flow field at a point for low void fraction, is expected to be intermittent in the sense that it is alternatively dominated by the original grid turbulence and turbulence associated with the velocity fields created by the moving bubbles. In the latter case velocities higher than in the surrounding flow prevail. This, causes an overall increase in the longitudinal flow velocity component affecting its probability distribution which becomes asymmetric acquiring a long skirt on the high velocity side and therefore positive skewness values. Furthermore, the velocity fluctuations due to the influence of the bubbles are characterised by higher intensities than the surrounding turbulence. The resulting succession of high and low turbulence intensity region is responsible for the observed flatness increase. As the void fraction increases, the buoyancy induced turbulence dominates, resulting in the intensification of turbulence convection responsible for the smoothing of the mentioned inhomogeneities. It is important to be recognised that this process is also responsible for the observed preferential increase of turbulence intensity in the longitudinal direction and contributes to the redistribution of the turbulence energy among the spectral wavelengths as will be discussed in the following.

4.4. Autocorrelation and spectra

Further information pertaining to the nature of the energy transfer processes, occurring between the turbulence field and the dispersed phase, can be obtained from the measured temporal autocorrelation and frequency spectra for different gas flow rate ratio, presented in Figs. 17–20. For the evaluation of the length scales involved in these processes, spatial autocorrelation and wave number power spectra of the longitudinal velocity at the centre of the channel were also computed by using Taylor's hypothesis as shown in Fig. 21. The low sampling rate prevented the calculation of temporal microscales. However, it is possible to have a rough estimate of their evolution by comparing the leading part of the autocorrelation graphs.

Regarding the bubble motion in the channel, it should be noted that the autocorrelation coefficient of bubble presence, R_b, as defined in the preceding discussion, measured at the centre of the channel and shown in Fig. 22, appears to fluctuate around the value ε_s, indicating randomness in the succession of bubbles. This implies, that there is no formation of an organised 'bubble structure' but, the bubbles are moving independently upwards. Moreover

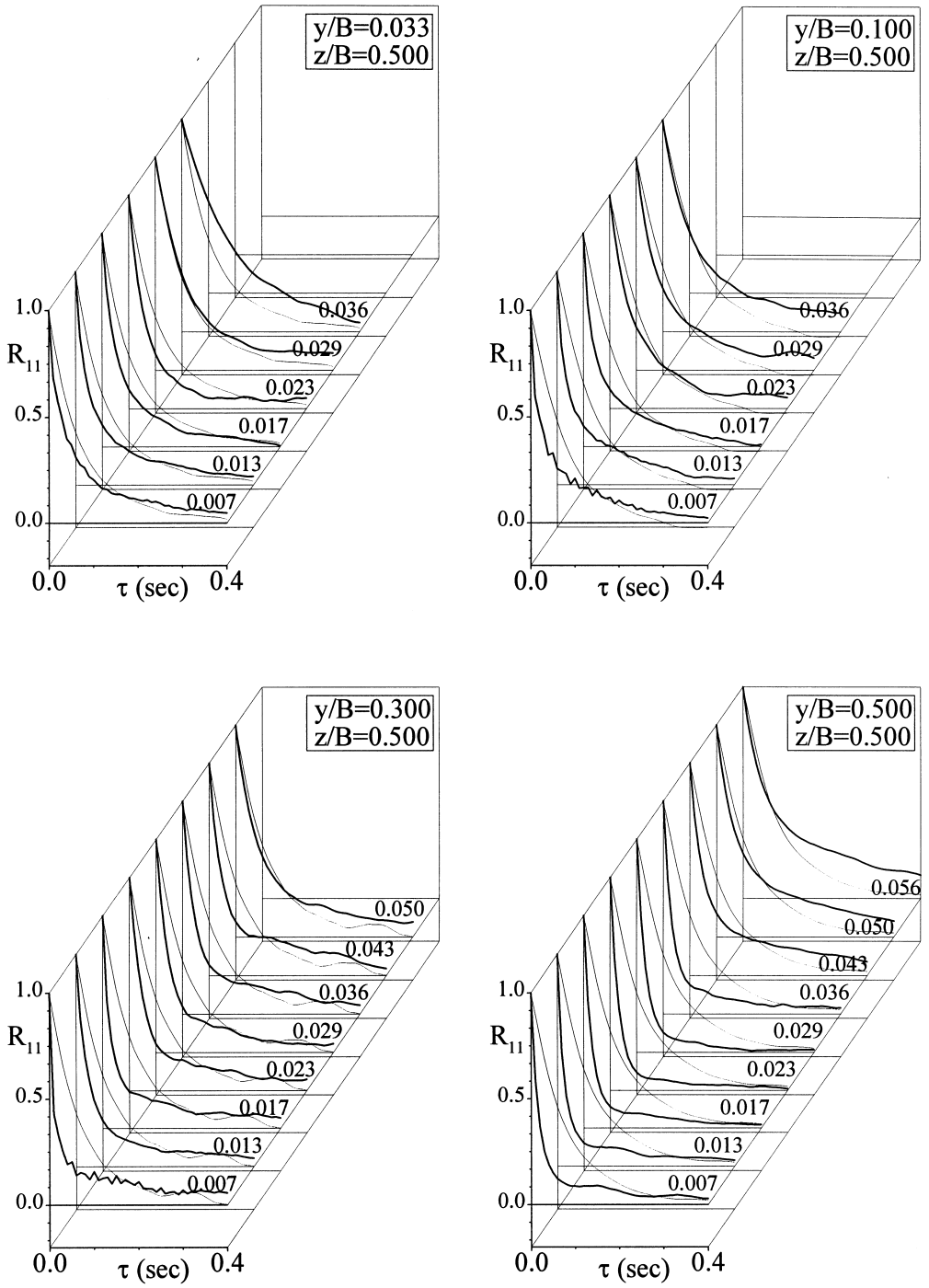

Fig. 17. Longitudinal autocorrelation for varying β (thin lines represent the corresponding single phase autocorrelation).

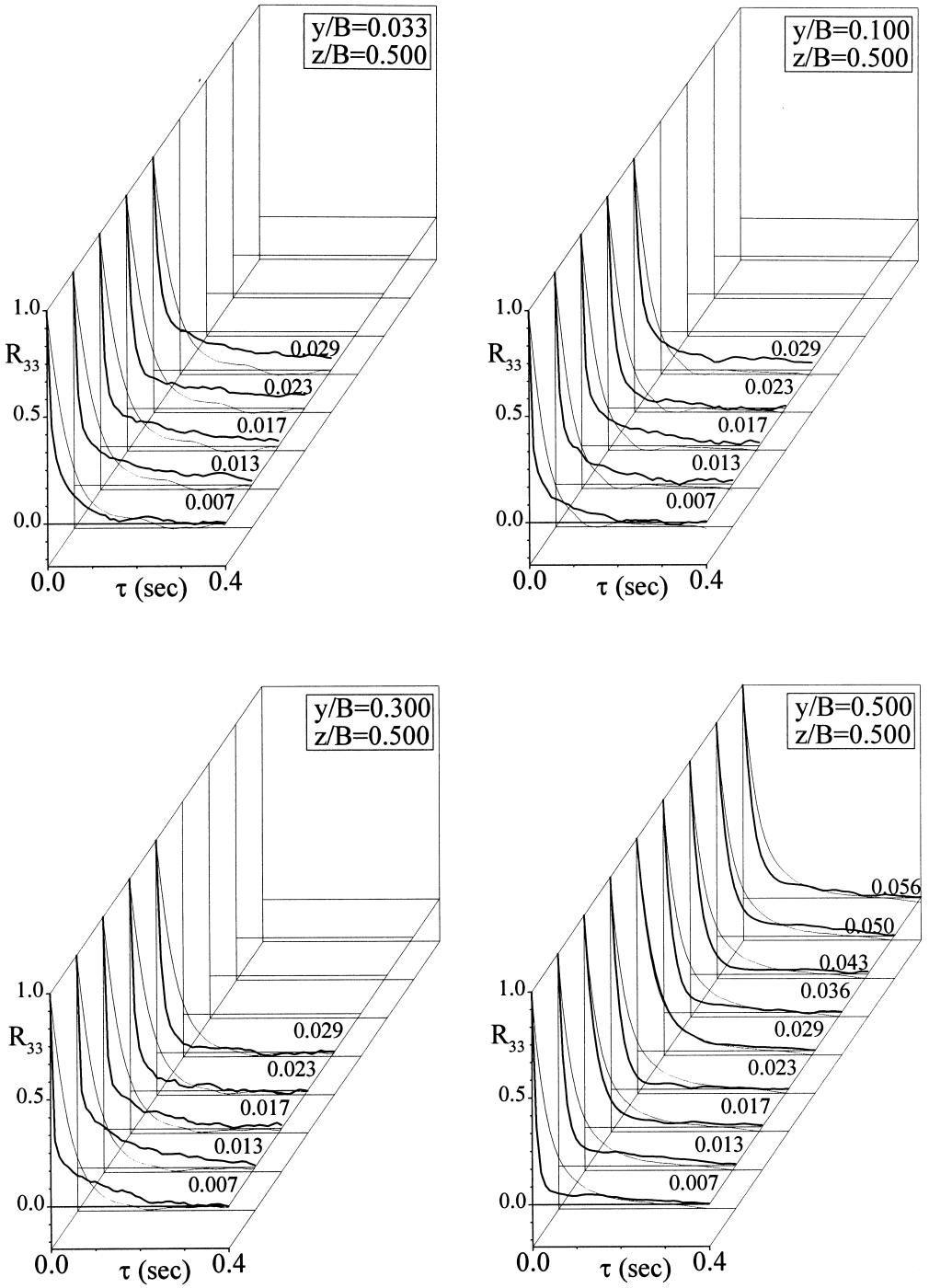

Fig. 18. Transverse autocorrelation for varying β (thin lines represent the corresponding single phase autocorrelation).

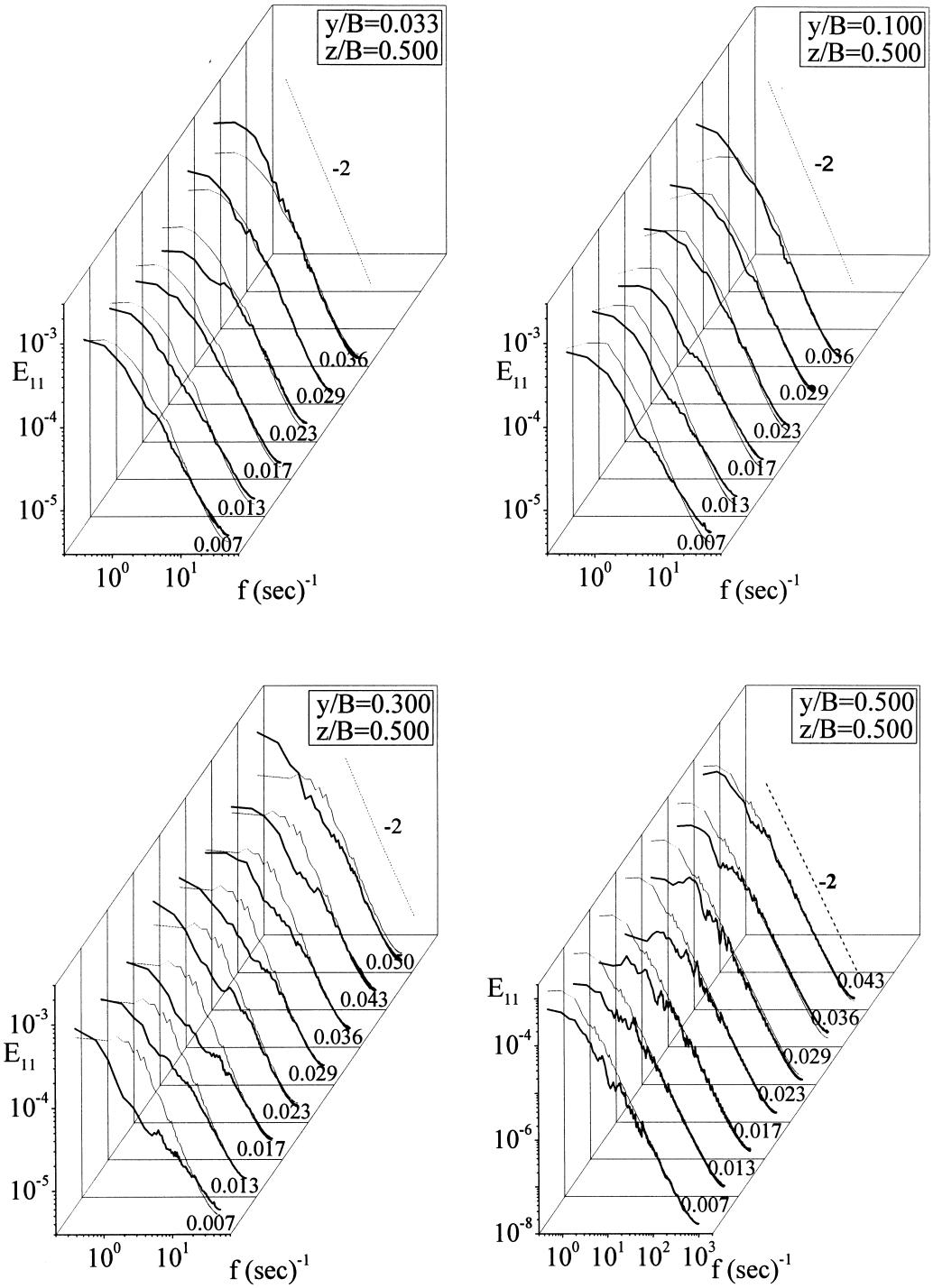

Fig. 19. Longitudinal power spectra for varying β (thin lines represent the corresponding single phase spectrum).

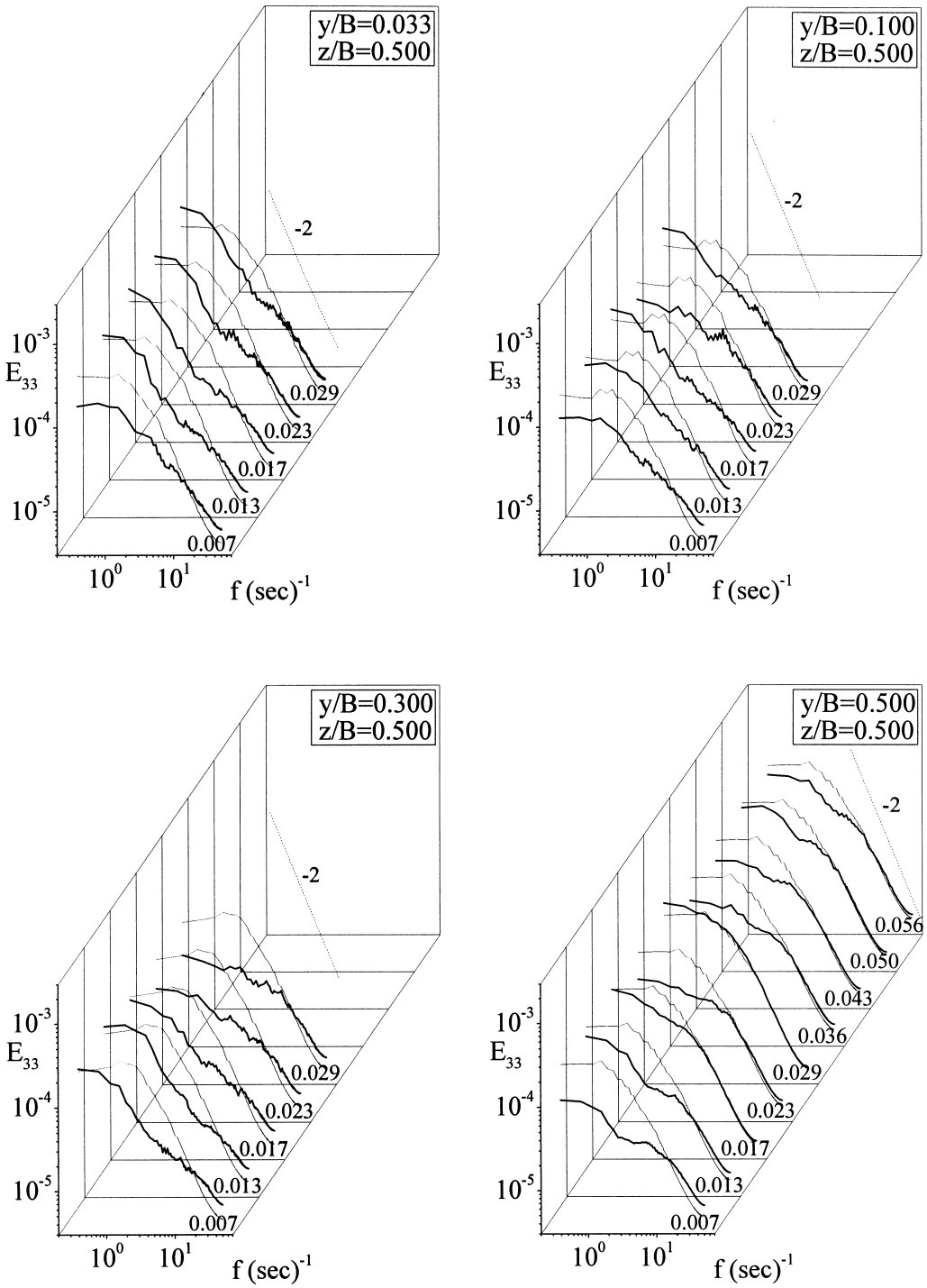

Fig. 20. Transverse power spectra for varying β (thin lines represent the corresponding single phase spectrum).

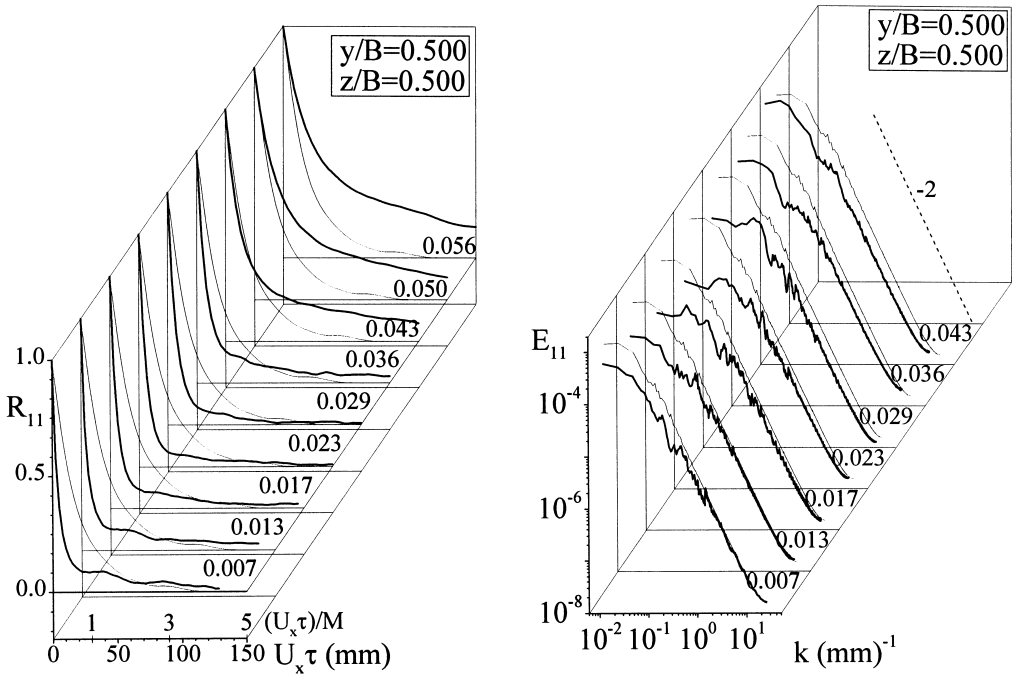

Fig. 21. Longitudinal spatial autocorrelation and wavenumber spectra at the centre of the channel for varying β (thin lines represent the corresponding single phase curve).

this means that the elimination of the water flow scales due to the presence of bubbles is evenly distributed in all scales and therefore the relative distribution of energy in the presented power spectra is not biased.

Consistent with the previously discussed statistical measurements, the succession of the

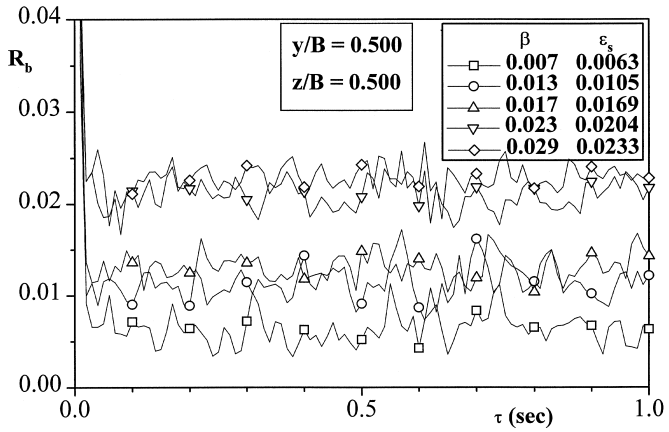

Fig. 22. Autocorrelation of bubble presence, at the centre of the test section.

structural changes imposed on the flow by the increasingly dominating presence of the dispersed phase are readily recognised in the obtained autocorrelation and power spectra.

The measured autocorrelation at low gas flow rates reconfirms the strong effect of the dispersed phase on the turbulence structure initiated with the injection of the bubbles. At the minimum gas flow rate ratio value of 0.007, a significant drop occurs in the autocorrelation affecting mainly its initial part, indicating a turbulence scale reduction. Inspection of the corresponding power spectra shown in Figs. 19 and 20 reveals that the presence of the bubbles affects the spectral distribution in the regions corresponding to medium and large scale eddies. The presented evidence can be contributed to the difference in the size between the single-phase grid turbulence eddies and the much smaller structures associated with the wake of the bubbles. Indeed the grid turbulence macroscale, estimated from the spatial autocorrelation was found approximately equal to 20 mm, while the characteristic size of the eddies produced by the moving bubbles is expected to be comparable to their mean diameter that is, approximately equal to 3 mm. The gradual change in the turbulence scales is also manifested by the appearance at low gas flow rate, of a slight hump located at the rear part of the autocorrelation which is more pronounced in those obtained at the centre of the channel. This, according to Townsend's (1976) interpretation, indicates the presence in the flow of a double turbulence structure consisting of two distinct ranges of eddy size namely, small eddies produced by the bubbles and larger eddies of the initial grid turbulence represented by the hump. Finally, it should be added that the observed scale reduction is more pronounced at the centre of the channel while it diminishes towards the walls.

As the gas flow rate increases the scale reduction continues at a much lower rate up to the mentioned gas flow rate ratio value of approximately 0.02. Thereafter a reverse trend is observed. For higher gas flow rate the scales of the flow are increased as the autocorrelation and spectra indicate. This should be attributed to the activation of an inverse energy cascade process due to the bubble forcing that is, the energy transferred from the bubbles to the mean flow at intermediate scales corresponding to their motion. This forcing becomes significant relatively to the mean flow energy, not entirely dissipated towards smaller scales but also redistributed to larger scales. Evidence of similar inverse cascade process has been predicted by direct numerical simulation studies for bubbly flows (Elghobashi and Truesdell, 1992; Esmaeeli and Tryggvason, 1996). Finally, the existence of a subrange characterised by a -2 power form should be noted in the high frequency region of all the obtained spectra. This finding is quite common in flows with a low Reynolds number (based on the root mean square velocity and the Taylor microscale) so that the smallest scales are not independent of the largest scales (Hunt and Carruthers, 1990). Since this form is observed to remain unaltered by the presence of the air–bubbles, it should be surmised that there is no interaction between the dispersed phase and the small scale turbulence eddies corresponding to this part of the power spectrum.

Differences with other common experimental findings such as a $-\frac{8}{3}$ power form and the absence of an inverse energy cascade indication (Lance and Bataille, 1991; Michiyoshi and Serizawa, 1986), should be probably attributed to the differences in the relation between the bubble forcing scales and the original single phase flow scales (especially the dissipation scales) and also to the significance of the bubble forcing in relation to the mean flow energy content at the corresponding stage of flow development.

5. Conclusions

Based on an overall interpretation of the experimental findings as presented in the preceding parts of this work, a summarising conclusion is given in the following.

Focusing attention mostly at the central part of the channel it can be concluded that the interfacial drag and the high bubble velocities have a direct effect on the water velocity field increasing significantly the mean velocities with gas flow rate. At low gas flow rate the bubble influence is intermittent leading to significant departure of the skewness and flatness values from these corresponding to a normal velocity distribution. At high gas flow rate the bubble influence dominate the flow and the PDF returns to a form close to that of a normal distribution. Fluctuations in the longitudinal direction are bounded at the low end by the single-phase velocity and at the high end by the total velocity of the bubbles which increase interactively with the mean velocity as the gas flow rate increases. Thus the turbulence intensity in the longitudinal direction is constantly increasing with the gas flow rate ratio. In the transverse directions the water velocity fluctuations are due to the bubble wakes and remain almost proportional to the mean flow keeping the transverse turbulence intensities almost constant with gas flow rate after a jump from single-phase flow. Due to this fact the isotropy of the flow field is inevitably destroyed.

Significant redistribution of void in the channel is observed resulting to the development of void and velocity peaks between the centre of the channel and the wall, more pronounced at high gas flow rate ratio values. This behaviour may be attributed to either the lift force acting on the bubbles due to the local shear or to the entrainment and capturing of the bubbles into large eddies developing in the channel. It can be stated, that the bubble motion establishes in the central part of the channel a free turbulence flow pattern, while a boundary layer of considerable thickness develops near the walls as a result of bubble–wall interaction.

Regarding the scales of the flow field the introduction of the bubbles at low gas flow rates results in a significant break up of the larger eddies. This trend is reversed after a specific gas flow rate ratio value is attained. For higher gas flow rate the bubble forcing that is, the energy transferred from the bubbles to the mean flow becomes significant relative to the mean flow energy content. This energy transfer at intermediate scales corresponding to the bubble motion cannot be entirely dissipated towards smaller scales but is redistributed to larger scales thus activating an inverse energy cascade process.

Finally as an assessment of the overall effect of the dispersed phase on the mean flow characteristics it can be stated, that two distinct regions corresponding to low and higher gas flow rate ratios have been identified. These regions which are clearly distinguished in the measurements of both the mean and statistical flow characteristics, are apparently associated with the existence of two different modes of interaction between the two phases, at low and high bubble concentration, related to changes in the balance among the acting forces.

Acknowledgements

The measurements of the development of void fraction for $Re = 7000$ have been accomplished with the help of Dr. Ziping Feng which we gratefully acknowledge.

References

Elghobashi, S., Truesdell, G.C., 1992. On the two-way interaction between homogeneous turbulence and dispersed solid particles. Part I: Turbulence modification. Phys. Fluids A 5, 1790–1801.

Ervin, E.A., Tryggvason, G., 1997. The rise of bubbles in a vertical shear flow. J. Fluids Eng 119, 443–449.

Esmaeeli, A., Tryggvason, G., 1996. An inverse energy cascade in two-dimensional low Reynolds number bubbly flows. J. Fluid Mech 314, 315–330.

Farrar, B., Bruun, H.H., 1989. Interaction effects between a cylindrical hot-film anemometer probe and bubbles in air/water and oil/water flows. J. Phys. E: Sci. Instrum 22, 114–123.

Gherson, P., Lykoudis, P.S., 1984. Local measurements in two-phase liquid–metal magneto-fluid-mechanic flow. J. Fluid Mech 147, 81–104.

Hunt, J.C.R., Carruthers, D.J., 1990. Rapid distortion theory and the 'problems' of turbulence. J. Fluid Mech 212, 497–532.

Kim, I., Elghobashi, S.E., Sirignano, W.A., 1993. Three dimensional flow over two spheres placed side by side. J. Fluid Mech 246, 465–488.

Lance, M., Bataille, J., 1982. Turbulence in the Liquid Phase of a Bubbly Air–water Flow. NATO Workshop, Shliersee.

Lance, M., Bataille, J., 1991. Turbulence in the liquid phase of a uniform bubbly air–water flow. J. Fluid Mech 222, 95–118.

Liu, T.J., 1997. Investigation of the wall shear stress in vertical bubbly flow under different bubble size conditions. Int. J. Multiphase Flow 23, 1085–1109.

Lopez de Bertodano, M., Lahey Jr, R.T., Jones, O.C., 1994. Phase distribution in bubbly two-phase flow in vertical ducts. Int. J. Multiphase Flow 20, 805–818.

Loth, E., Taeibi-Rahni, M., Tryggvason, G., 1997. Deformable bubbles in a free shear layer. Int. J. Multiphase Flow 23, 977–1001.

Mahalingam, R., Limaye, R.S., Brink Jr, J.A., 1976. Velocity measurements in two-phase bubble-flow regime with laser-Doppler anemometry. AIChE J 22, 1152–1155.

Marie, J.L., 1983. Investigation of two-phase bubbly flows using laser Doppler anemometry. Pch J 4, 103–118.

Marie, J.L., Lance, M., 1984. Turbulence measurements in two-phase bubbly flows using laser Doppler anemometry. In: Measuring Techniques in Gas-Liquid Two-Phase Flows. Springer, Berlin, pp. 141–148.

Marie, J.L., Moursali, E., Tran-Cong, S., 1997. Similarity law and turbulence intensity profiles in a bubbly boundary layer at low void fractions. Int. J. Multiphase Flow 23, 227–247.

Michiyoshi, I., Serizawa, A., 1986. Turbulence in two-phase bubbly flow. Nuc. Eng. Design 95, 253–267.

Moursali, E., Marie, J.L., Bataille, J., 1995. An upward turbulent bubbly boundary layer along a vertical flat plate. Int. J. Multiphase Flow 21, 107–117.

Nakoryakov, V.E., Kashinsky, O.N., Burdukov, A.P., Odnoral, V.P., 1981. Local characteristics of upward gas liquid flows. Int. J. Multiphase Flow 7, 63–81.

Panidis, Th., 1995. On the evaluation of autocorrelation and power spectrum in dispersed two phase flows. In: Proc. of the Int. Symp. on Measuring Techniques for Multiphase Flows, Nanjing, 275–280.

Panidis, Th., 1996. Correction factor for void fraction measurements with a line sensor. In: Advances in Turbulence VI. Kluwer Academic publishers, Dordrecht, pp. 571–572.

Panidis, Th., Sommerfeld, M., 1997. The locus of centres method for LDA and PDA measurements. In: Developments in Laser Techniques and Fluid Mechanics. Springer–Verlag, Berlin (Selected Papers from the 8th International Symposium).

Segre, G., Silberberg, A., 1962. Behaviour of macroscopic rigid spheres in Poiseuille flow (Parts 1/2). J. Fluid Mech 14, 115–157.

Serizawa, A., 1974. Fluid-dynamic characteristics of two-phase flow. Thesis, Institute of Atomic Energy, Kyoto.

Serizawa, A., Kataoka, I., Michiyoshi, I., 1975. Turbulence structure of air–water bubbly flow (Parts I–III). Int. J. Multiphase Flow 2, 221–259.

Serizawa, A., Tsuda, K., Michiyoshi, I., 1984. Real-time measurements of two-phase flow turbulence using a dual-sensor anemometry. In: Measuring Techniques in Gas–Liquid Two-Phase Flows. Springer–Verlag, Berlin, pp. 495–523.

Sim, S.K., Lahey Jr, R.T., 1986. Measurement of phase distribution in a triangular conduit. Int. J. Multiphase Flow 12, 105–425.

Stewart, R.W., 1951. Triple velocity correlations in isotropic turbulence. Proc. Cambridge Phil. Soc 47, 146–157.

Theofanous, T.G., Sullivan, J., 1982. Turbulence in two-phase dispersed flows. J. Fluid Mech 116, 343–362.

Tomiyama, A., Sou, A., Zun, I., Kanami, N., Sakaguchi, T., 1995. Effects of Eotvos number and dimensionless liquid volumetric flux on lateral motion of a bubble in a laminar duct flow. In: Proc. of the 2nd Int. Conf. on Multiphase Flow, Kyoto, PD1.11–18.

Townsend, A.A., 1976. The Structure of Turbulent Shear Flow. Cambridge University Press, Cambridge.

Tsuji, Y., Morikawa, Y., 1982. LDV measurements of an air–solid two-phase flow in horizontal pipe. J. Fluid Mech 120, 385–409.

van Atta, C.W., Chen, W.Y., 1968. Correlation measurements in grid turbulence using digital harmonic analysis. J. Fluid Mech 34, 497–515.

van Atta, C.W., Chen, W.Y., 1969. Measurements of spectral energy transfer in grid turbulence. J. Fluid Mech 38, 743–763.

Wang, S.K., Lee, S.J., Jones Jr, O.C., Lahey Jr, R.T., 1987. 3D turbulence structure and phase distribution measurements in bubbly two-phase flows. Int. J. Multiphase Flow 13, 327–343.